S1 Simulation studies

The following two simpler simulation cases have also been developed for the simulation study, including only one source with and without a constant source outside the inversion domain.

– Case 1: a single source in slurry pit A3 with a linearly increasing emission rate.

5 – Case 2: similar to Case 1, with the added complexity of another constant source outside the inversion computational domain. This case is designed to evaluate the sensitivity of the inversion's accuracy to the intrusion of gas transported from external sources that cross-contaminates the PAC measurements.

S1.1 Case 1 - single emission source

From columns 1 to 6, Figure S1 shows snapshots of temporal evolutions of: i) the true concentration in ppm, ii) the estimated
10 one using the unconstrained model, iii) the estimated one using the constrained model, iv) the true source distribution in g h^{-1}, v) the estimated one using the unconstrained model, and vi) the estimated one using the constrained model. The concentration and source distributions are illustrated at times instants 15, 30, 45, and 60 min of the simulations (rows).

The reconstructed concentration distributions in Fig. S1 using the unconstrained and constrained source models (second and third columns) show good correspondence with the true concentration distribution (first column). The reconstructed gas plumes
15 capture the transport of gas in the direction of the velocity field marked with green vectors. In the second row of Fig. S1, the reconstructed concentration and source distributions show that the unconstrained model (fifth column) detects the source in slurry pit A3 later than the constrained model (sixth column). After the initial delay, the unconstrained model localizes the source well to the correct slurry pit.

Figure S2 shows the corresponding integrated source distributions as time-evolving emission rates with 95 % posterior
20 credibility intervals for the unconstrained (top) and the constrained source model (bottom). For the unconstrained source model, the 95 % posterior credibility intervals contain the true integrated emission rate about 40 % of the time. For the constrained source model (top right), the true integrated emission rate is estimated within the 95 % posterior credibility intervals at all times. The reconstructions show that the constrained source model performs better than the unconstrained one, yielding faster detection and more accurate quantification.

25 Figure S3 shows the simulated (red) vs. estimated (black) path-averaged concentration (PAC) measurements for case 1 using the constrained source model (unconstrained model left out for brevity). The figure shows how the reflectors downwind of the sources (R1-R3) do not detect any elevated concentrations, since the wind directions transported the gas in the opposite direction. The simulated concentration measurements are reconstructed well by the constrained model.

S1.2 Case 2 - single source with external input

30 Figure S4 shows the true and reconstructed concentration and source distributions for case 2. In this simulation case, we simulate the forward problem in an expanded version of the FE mesh used for the inversion, such that a source can be placed outside the modeled domain of interest. We denote sources located outside the inversion domain as external sources. The wind field transports the gas emitted from the external source into the area of interest. This way, the externally emitted gas cross-contaminates the PAC measurements of any sources inside the inversion domain. The green squares in the true concentration
35 and source distributions (first and fourth columns) of Fig. S3 represent the boundaries of the inversion domain. Since gas enters the inversion domain through the input boundary, we increase the standard deviation of the stochastic input boundary term to 1.5 ppm. Increasing the uncertainty of the stochastic input boundary condition gives the model more flexibility to capture boundary variations, such as gas entering the domain.

The estimated concentration distribution in Fig. S4 shows that the unconstrained source model (second column) is unable to
40 reconstruct the gas entering the domain through the input boundary from the external source. The estimated source distribution from the unconstrained model (fifth column) shows that the model does not detect the true source. Instead, the unconstrained model explains the gas coming in through the input boundary by creating false sources near the input boundary. These results show that the unconstrained source model performs poorly when external sources cross-contaminate the measured concentration data.
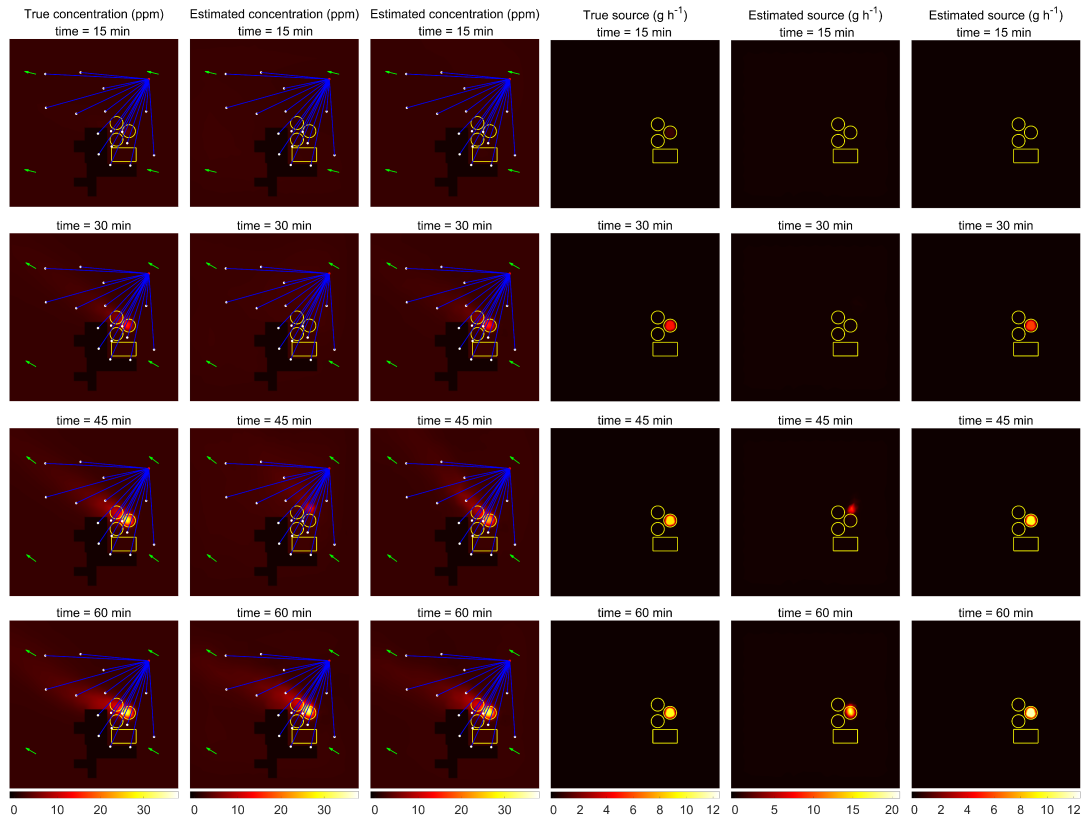
Figure S1. Case 1 - First column) true concentration distribution at different time instants. The wind direction at each time is shown with green vectors. Second column) estimated concentration distribution using the unconstrained model. Third column) estimated concentration distribution using the constrained model. Fourth column) true source distribution. Fifth column) estimated source distribution using the unconstrained model. Sixth column) estimated source distribution using the constrained model.

The reconstructed concentration distribution from the constrained source model in Fig. S4 (third column) shows gas entering the domain through the input boundary, even before the source in slurry pit A3 is active (first row). The constrained source model correctly detects that none of the source locations A1-A4 can reproduce the measured concentration data. Therefore, the concentration data must be explained by some boundary variations, which is correct for this simulation case. The corresponding reconstructed source distribution (sixth column) shows no source until 30 minutes, but after this, the source in slurry pit A3 is reconstructed well. This simulation case highlights how the constrained source evolution model effectively mitigates the impact of external gas sources, avoiding spurious sources near the boundary. The bottom row of Fig. S2 shows the estimated integrated emission rates from the unconstrained (left) and constrained (right) source evolution models. The constrained source model detects the source after 15-20 minutes, while the true source appears after 12 minutes. The constrained source model gives a good estimate of the integrated emission rate, and the true integrated emission rate is contained within the 95 % posterior credible intervals most of the time. The unconstrained source model, however, gives a very poor estimate due to its inability to handle gas entering the inversion domain through the input boundary.

By comparing the synthetic PAC measurements in Fig. S3 from simulation case 1 to the PAC measurements in Fig. S5 from simulation case 3, it can be seen how the external source has contaminated the PAC measurements in case 3. In Fig. S3 for case 1, the peak PAC measurement is ∼5 ppm, while the peak PAC measurement for case 3 in Fig. S5 is ∼15 ppm.
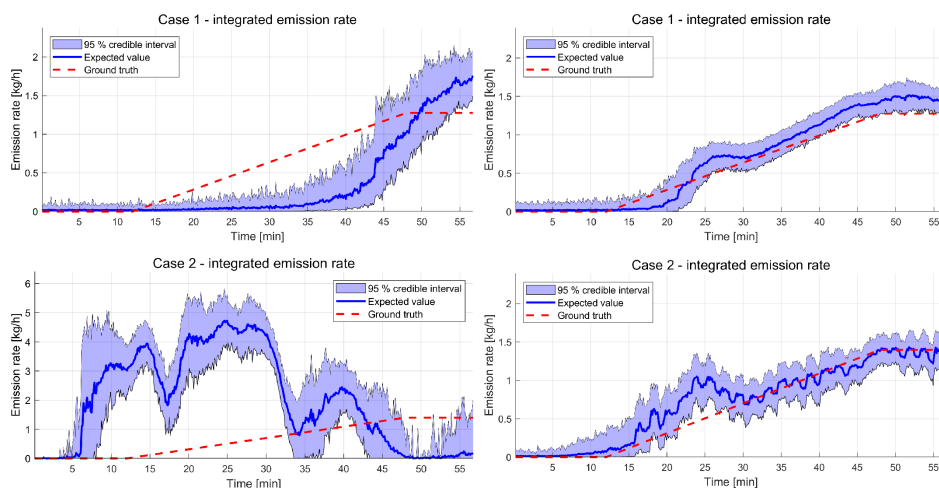
Figure S2. Integrated source distributions in kg h⁻¹ for the supplementary simulation cases using the unconstrained (left column) and the constrained source evolution models (right column).
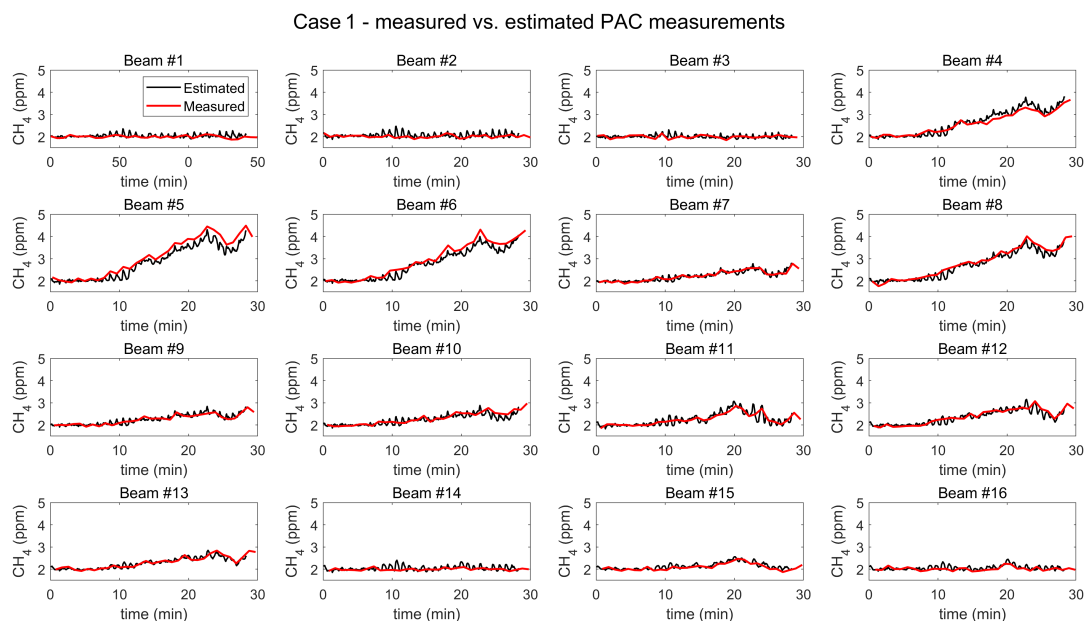
Figure S3. Case 1 - Measured (from forward simulation) and estimated (from inversion) PAC measurements using the constrained model.

S2   Experimental campaign - slurry pumping and agitation

Agitating or pumping animal slurry releases trapped methane bubbles and promotes methane emissions from the slurry. Agitation with a slurry agitator is necessary to prevent the formation of a crust on top of the slurry, since the slurry tends to form floating layers during prolonged storage. During the slurry agitation event on 9 May, the slurry was mixed with a tractor-driven slurry agitator as shown to the left in Fig. S6. Pumping of animal slurry between slurry pits can be necessary when only one of the pits is connected to the animal barn where the slurry comes from, and more storage space is needed. During the slurry
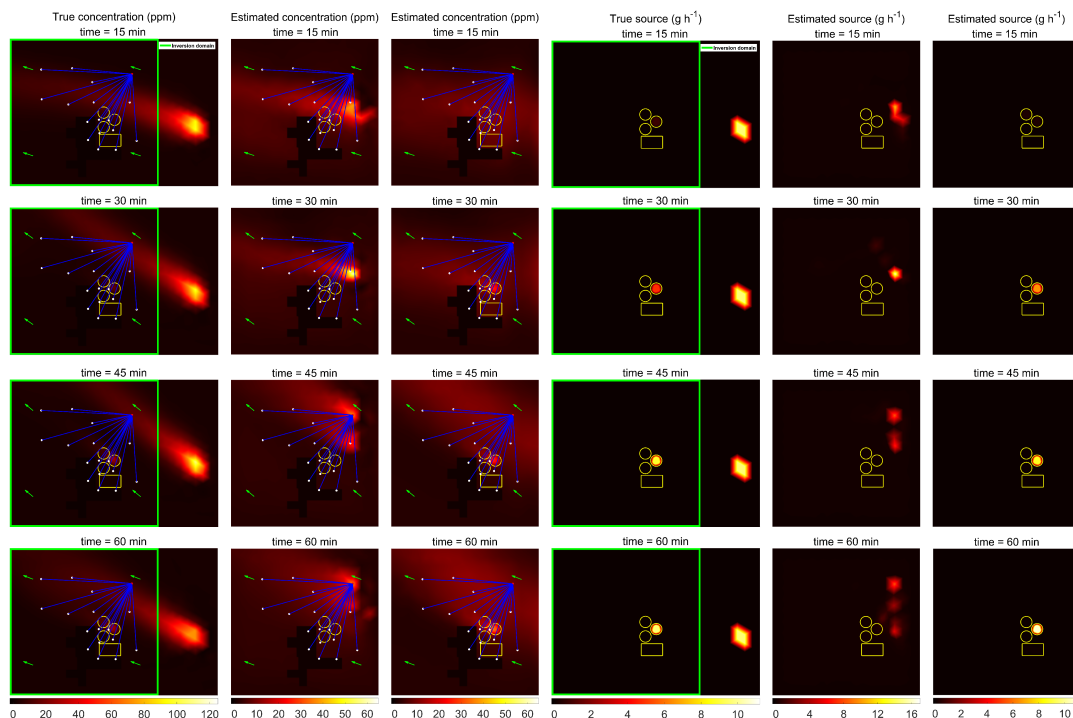
Figure S4. Case 2 - First column) true concentration distribution at different time instants. The green square is the inversion domain. Second column) estimated concentration distribution using the unconstrained model. Third column) estimated concentration distribution using the constrained model. Fourth column) true source distribution. Fifth column) estimated source distribution using the unconstrained model. Sixth column) estimated source distribution using the constrained model.

pumping event on 22 May, the slurry was pumped with enough force to splash down onto the surface of the slurry already in the tank, causing significant mechanical agitation as shown to the right in Fig. S6.
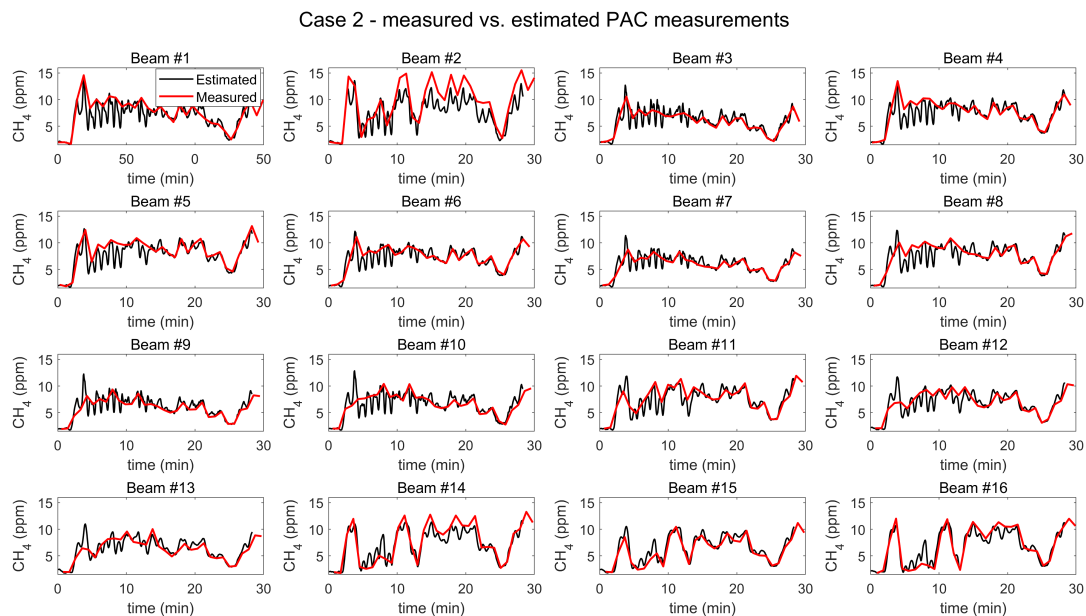
Figure S5. Case 2 - Measured (from forward simulation) and estimated (from inversion) PAC measurements using the constrained model.

Figure S6. (Left) Picture of the slurry agitation event on 9 May 2023. The slurry is mixed with a tractor-operated slurry agitator, releasing trapped methane bubbles to the atmosphere. (Right) Picture of the slurry pumping event on 22 May 2023. The slurry is pumped from pit A1 to A3, with enough pressure to cause mechanical agitation of the slurry.